Study correlation vortices in the near-field of partially coherent vortex beams diffracted by an aperture*

Li Jian-Long(李建龙)†

College of Physics Science and Technology, Sichuan University, Chengdu 610064, *China*

(Received 20 December 2009; revised manuscript received 24 May 2010)

We have derived the analytical expression of the electric cross-spectral density in the near- field of partially coherent vortex beams diffracted by an aperture. Taking the Gaussian Schell-model vortex beam as a typical example of partially coherent vortex beams, the spatial correlation properties and correlation vortices in the near-field of partially coherent vortex beams diffracted by a rectangle aperture are studied. It is shown that the off-axis displacement, spatial degree of coherence parameter, propagation distance, and the opening factor of the aperture affect the spectral degree of coherence and positions of correlation vortices. With the optimization algorithm, we obtain the symmetric distributing coherent vortex.

Keywords: spatial correlation property, correlation vortex, aperture diffraction, near-field

PACC: 4000, 4225B

1. Introduction

Much interest has been exhibited in singular optics, which primarily dealt with fully coherent, quasi-monochromatic beams,[1,2] and has recently been extended to fully coherent, polychromatic beams,[3,4] as well as partially coherent, quasi-monochromatic beams.[5−10] Many investigations have been carried out concerning correlation vortices of the partially coherent beams.[7−11] However, to our knowledge, practically no studies have been made as to spatial correlation properties and correlation vortices in the near-field of partially coherent vortex beams diffracted by an aperture. The main part of this paper is concerned with this question. The consideration of this problem has considerable importance, because its results may be ultimately for the study of the features and control of the spatial correlation properties and correlation vortices in the near-field or other sub-wavelength zone. In Section 2, by using the Simpson's rule, analytical expressions for the cross spectral density and spectral degree of coherence of a Gaussian Schell model (GSM) vortex beam diffracted by an aperture are derived and analysed. The spatial correlation properties and dependence of correlated vortices on the beam and aperture parameters and propagation distance are studied and illustrated by numerical examples in Section 3. Finally, Section 4 summarizes the main results obtained in this paper.

2. Correlation vortices in the near-field diffraction region

Consider a stochastic (random), statistically stationary, electromagnetic beam propagating through the aperture lens system. Let $\boldsymbol{E}(\boldsymbol{r}_{10},\omega)$ ($\boldsymbol{r}_{10} = x_{10}\boldsymbol{i} + y_{10}\boldsymbol{j}, \boldsymbol{i}$, $\boldsymbol{j}$ and $\boldsymbol{k}$ represent the unit vectors of the x, y and z axes, respectively) be a statistical ensemble of the fluctuating components of frequency ω of the electric field at the plane $z = 0$.[12] Suppose that an opaque screen P_1, with a small opening at point $P_1(A)$, is placed across the beam, perpendicular to the z direction, and that the interference pattern, formed by the beam emerging from the aperture, is observed in a plane P_2, placed some distance behind the convergence lens f and parallel to it (as shown in Fig. 1). Regions I, II and III denote the incidence region, aperture diffraction region and lens convergence region, respectively. The distances between lens and diffraction screen, between lens and observation screen are s_0 and s_1, respectively. The electric field $\boldsymbol{E}(\boldsymbol{r}_1, \omega)$ in region II can be obtained with the electric field $\boldsymbol{E}(\boldsymbol{r}_{10}, \omega)$ propagating through the aperture $p_1(A)$ by means of the Rayleigh–Sommerfeld diffraction theory.[13] That

*Project supported by the China Postdoctoral Science Foundation (Grant No. 2009450159) and the Foundation of the State Key Laboratory of Optical Technologies for Micro-Frabrication & Micro-Engineering, Chinese Academy of Sciences (Grant No. KF001).

†Corresponding author. E-mail: sculjl@163.com

© 2010 Chinese Physical Society and IOP Publishing Ltd

is,

$$\boldsymbol{E}(\boldsymbol{r}_1,\omega) = \frac{1}{2\pi}\iint_{P_1}\boldsymbol{E}(\boldsymbol{r}_{10},\omega)\frac{z_1}{R_1^3}(1-\mathrm{i}kR_1) \times \exp(\mathrm{i}kR_1)\,\mathrm{d}x_{10}\,\mathrm{d}y_{10}, \quad (1)$$

where $\boldsymbol{r}_1 = x_1\boldsymbol{i} + y_1\boldsymbol{j} + z_1\boldsymbol{k}$, $R_1 = [(x_1 - x_{10})^2 + (y_1 - y_{10})^2 + z_1^2]^{1/2}$.

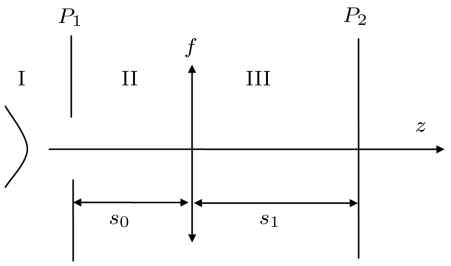


Fig. 1. Schematic diagram of the aperture and lens.

Similarly, the electric field $\boldsymbol{E}(\boldsymbol{r}_2, \omega)$ in region II can be obtained with the electric field $\boldsymbol{E}(\boldsymbol{r}_{20}, \omega)$ propagating through the aperture $P_1(A)$ by means of the Rayleigh–Sommerfeld diffraction theory, and written as

$$\boldsymbol{E}(\boldsymbol{r}_2,\omega) = \frac{1}{2\pi}\iint_{P_1}\boldsymbol{E}(\boldsymbol{r}_{20},\omega)\frac{z_1}{R_2^3}(1-\mathrm{i}kR_2) \times \exp(\mathrm{i}kR_2)\,\mathrm{d}x_{20}\,\mathrm{d}y_{20}, \quad (2)$$

where $\boldsymbol{r}_2 = x_2\boldsymbol{i} + y_2\boldsymbol{j} + z_2\boldsymbol{k}$, $R_2 = [(x_2 - x_{20})^2 + (y_2 - y_{20})^2 + z_2^2]^{1/2}$.

According to the definition of the electric cross-spectral density, we have

$$W(\boldsymbol{r}_1,\boldsymbol{r}_2,\omega) = \langle\boldsymbol{E}(\boldsymbol{r}_1,\omega)\boldsymbol{E}^*(\boldsymbol{r}_2,\omega)\rangle, \quad (3)$$

where $\langle\ \rangle$ and $*$ denote the time ensemble average with respect to time and the complex conjugate, respectively. Substituting Eqs. (1) and (2) into Eq. (3), the cross-spectral density of the electric field at the plane z in region II is given by

$$W^{(2)}(\boldsymbol{r}_1,\boldsymbol{r}_2,\omega) = \iint_{P_1} W^{(1)}(\boldsymbol{r}_{10},\boldsymbol{r}_{20},\omega)F(\boldsymbol{r}_{10},\boldsymbol{r}_{20},\boldsymbol{r}_1,\boldsymbol{r}_2,\omega)\,\mathrm{d}\boldsymbol{r}_{10}\,\mathrm{d}\boldsymbol{r}_{20}, \quad (4)$$

where

$$F(\boldsymbol{r}_{10},\boldsymbol{r}_{20},\boldsymbol{r}_1,\boldsymbol{r}_2,\omega) = \frac{z_1 z_2}{R_1^3 R_2^3}(1-\mathrm{i}kR_1)(1+\mathrm{i}kR_2)\exp[\mathrm{i}k(R_1-R_2)]\,\mathrm{d}\boldsymbol{r}_{10}\,\mathrm{d}\boldsymbol{r}_{20}, \quad (4a)$$

$$W^{(1)}(\boldsymbol{r}_{10},\boldsymbol{r}_{20},\omega) = \langle\boldsymbol{E}^*(\boldsymbol{r}_{10},\omega)\boldsymbol{E}(\boldsymbol{r}_{20},\omega)\rangle \quad (4b)$$

with $k = 2\pi/\lambda$. Equations (4a) and (4b) denote the propagation factor of the electromagnetic field and the cross-spectral density of the electromagnetic field at the plane $z = 0$, respectively. We present in this paper a powerful numerical method for evaluation of the diffraction integral Eq. (4). The numerical method is based upon a product integration rule in which Simpson's 1/3 rule is applied four times. This method can give accurate results in reasonable time intervals with a PC computer and with a software program such as Matlab.[14]

From Eq. (4), we know that the integrals to be evaluated for the electric cross-spectral density in the diffracted wave field are of the form

$$W^{(2)}(\boldsymbol{r}_1,\boldsymbol{r}_2,\omega) = \iiiint_{\text{aperture}} f(\boldsymbol{r}_{10},\boldsymbol{r}_{20},\boldsymbol{r}_1,\boldsymbol{r}_2,\omega)\,\mathrm{d}\boldsymbol{r}_{10}\,\mathrm{d}\boldsymbol{r}_{20}, \quad (4c)$$

and the integration can be done quickly and accurately using the product-integration rule.[15]

Now, divide the diffraction aperture $P_1(A)$ along the x and y directions into $M \times N$ grids, and the Δx, Δy subdivision step lengths along the x and y axes are

$$\Delta x = \frac{a_1 - a_2}{M}, \quad \Delta y = \frac{b_1 - b_2}{N}, \quad (5)$$

where $x_s \in (a_1, a_2)$ and $y_s \in (b_1, b_2)$ denote the open regions of the aperture along the x and y directions, respectively. Then equation (4) can be evaluated by the Simpson's 1/3 rule. The rule is based on a quadratic polynomial approximation to function $f(\boldsymbol{r}_{10}, \boldsymbol{r}_{20}, \boldsymbol{r}_1, \boldsymbol{r}_2, \omega)$ over a pair of partitions. $M-1$ and $N-1$ are the numbers of partitions, where M and N must be odd and so equation (4) can be rewritten as

$$W^{(2)}(\boldsymbol{r}_1,\boldsymbol{r}_2,\omega) = \frac{\Delta y}{3}\{F_3(b_1;\boldsymbol{r}_1,\boldsymbol{r}_2,\omega) + F_3(b_2;\boldsymbol{r}_1,\boldsymbol{r}_2,\omega) + 4F_3[(b_1+(2n-1)\Delta y);\boldsymbol{r}_1,\boldsymbol{r}_2,\omega] + 2F_3[(b_1+2n\Delta y);\boldsymbol{r}_1,\boldsymbol{r}_2,\omega]\}, \quad (6)$$

where

$$F_3(y_{20};\boldsymbol{r}_1,\boldsymbol{r}_2,\omega) = \frac{\Delta x}{3}\{F_2(a_1,y_{20};\boldsymbol{r}_1,\boldsymbol{r}_2,\omega) + F_2(a_2,y_{20};\boldsymbol{r}_1,\boldsymbol{r}_2,\omega) + 4F_2[(a_1+(2m-1)\Delta x),y_{20};\boldsymbol{r}_1,\boldsymbol{r}_2,\omega] + 2F_2[(a_1+2m\Delta x),y_{20};\boldsymbol{r}_1,\boldsymbol{r}_2,\omega]\}, \quad (7a)$$

$$F_2(x_{20},y_{20};\boldsymbol{r}_1,\boldsymbol{r}_2,\omega) = \frac{\Delta y}{3}\{F_1(b_1,\boldsymbol{r}_{20};\boldsymbol{r}_1,\boldsymbol{r}_2,\omega) + F_1(b_2,\boldsymbol{r}_{20};\boldsymbol{r}_1,\boldsymbol{r}_2,\omega) + 4F_1[(b_1+(2n-1)\Delta y),\boldsymbol{r}_{20};\boldsymbol{r}_1,\boldsymbol{r}_2,\omega] + 2F_1[(b_1+2n\Delta y),\boldsymbol{r}_{20};\boldsymbol{r}_1,\boldsymbol{r}_2,\omega]\}, \quad (7b)$$

$$F_1(y_{10},\boldsymbol{r}_{20};\boldsymbol{r}_1,\boldsymbol{r}_2,\omega) = \frac{\Delta x}{3}\{F(a_1,y_{10},\boldsymbol{r}_{20};\boldsymbol{r}_1,\boldsymbol{r}_2,\omega) + F(a_2,y_{10},\boldsymbol{r}_{20};\boldsymbol{r}_1,\boldsymbol{r}_2,\omega) + 4F[(a_1+(2m-1)\Delta x),y_{10},\boldsymbol{r}_{20};\boldsymbol{r}_1,\boldsymbol{r}_2,\omega] + 2F[(a_1+2m\Delta x),y_{10},\boldsymbol{r}_{20};\boldsymbol{r}_1,\boldsymbol{r}_2,\omega]\}. \quad (7c)$$

Here n and m are natural numbers, and $1 \le m \le M$, $1 \le n \le N$.

Based on Eq. (4a), and gradually utilizing Eqs. (7a), (7b), and (7c), we can obtain Eq. (6). This is the summarization form translated from the Rayleigh–Sommerfeld diffraction integration formula; this form has finite terms, and promises a fast calculation speed and a good accuracy.

Substituting Eq. (4) into the Collins formula, which denotes the electric cross-spectral density propagating through convergence lens f of the partially coherent light, we can obtain the electric cross-spectral density in region III

$$W^{(3)}(\boldsymbol{r}_{11},\boldsymbol{r}_{22},\omega) = \left(\frac{1}{\lambda B}\right)^2 \iint W^{(2)}(\boldsymbol{r}_1,\boldsymbol{r}_2,\omega)\exp\left\{\frac{\mathrm{i}k}{2B}[A(\boldsymbol{r}_2^2-\boldsymbol{r}_1^2)+D(\boldsymbol{r}_{22}^2-\boldsymbol{r}_{11}^2)+2(\boldsymbol{r}_2\cdot\boldsymbol{r}_{22}-\boldsymbol{r}_1\cdot\boldsymbol{r}_{11})]\right\}\mathrm{d}\boldsymbol{r}_{11}\,\mathrm{d}\boldsymbol{r}_{22}, \quad (8)$$

where λ is the wavelength of the incident beam, $\boldsymbol{r}_{vv} = x_{vv}\boldsymbol{i} + y_{vv}\boldsymbol{j} + z_{vv}\boldsymbol{k}$ $(v = 1, 2)$. And A, B, C, and D can be obtained by the matrix below (as shown in Fig. 1)

$$\begin{bmatrix} A & C \\ B & D \end{bmatrix} = \begin{bmatrix} 1 & s_1 \\ 1 & 1 \end{bmatrix}\begin{bmatrix} 1 & 0 \\ -1/f_1 & 1 \end{bmatrix}\begin{bmatrix} 1 & s_0 \\ 0 & 1 \end{bmatrix} = \begin{bmatrix} 1-s_1/f_1 & s_1+s_0-s_1s_0/f_1 \\ -1/f_1 & 1-s_1/f_1 \end{bmatrix}, \quad (9)$$

where f_1 is the focus distance of the lens f. Substituting the electric cross-spectral density expressed as Eq. (6) into Eq. (8), we obtain the electric cross-spectral density in region III.

The spectral degree of coherence at the plane z can be expressed as

$$\mu(\boldsymbol{r}_1,\boldsymbol{r}_2,\omega) = \frac{W(\boldsymbol{r}_1,\boldsymbol{r}_2,\omega)}{\sqrt{W(\boldsymbol{r}_2,\boldsymbol{r}_2,\omega)}\sqrt{W(\boldsymbol{r}_1,\boldsymbol{r}_1,\omega)}}. \quad (10)$$

The position of correlation vortices is given by

$$\mathrm{Re}[\mu(\boldsymbol{r}_1,\boldsymbol{r}_2,\omega)] = 0, \quad \mathrm{Im}[\mu(\boldsymbol{r}_1,\boldsymbol{r}_2,\omega)] = 0, \quad (11)$$

where Re and Im denote the real and imaginary parts of $\mu(\boldsymbol{r}_1,\boldsymbol{r}_2,\omega)$, respectively. The topological charge and its sign of correlation vortices are determined by the vorticity of phase contours around singularities.[16]

3. A typical example: spatial coherence and coherent vortex of Gaussian Schell model (GSM) vortex beams diffracted by a rectangular aperture

The field of optical vortex beam at the source plane $z = 0$ in the Cartesian coordinate system is given by[9]

$$E(x,y,0) = f(x,y)A(x',y')\exp[\mathrm{i}m\arctan(y'/x')]\exp(\mathrm{i}\Psi), \quad (12)$$

where $\boldsymbol{r} = (x,y)$ and $\boldsymbol{r}' = (x',y')$ denote coordinates of the beam and vortex core, respectively, and the vectors $\boldsymbol{r}$ and $\boldsymbol{r}'$ are related to the displacement vector $\boldsymbol{d}$ by $\boldsymbol{r} = \boldsymbol{r}' + \boldsymbol{d}$; $f(x,y)$ denotes the profile of the beam envelope, $A(x',y')$ is the vortex core function, m is the topological charge, and Ψ is an arbitrary phase.

Assume that the statistical distribution of β corresponds to a Schell-model correlator,[8,9] i.e.

$$C\left(|x_1-x_2|,|y_1-y_2|\right) = \exp\left(-\frac{(x_1-x_2)^2+(y_1-y_2)^2}{\sigma_0^2}\right), \quad (13)$$

where σ_0 is the spatial correlation length.

From Eqs. (12), (13), and (4b), the cross-spectral density function of a partially coherent vortex beam at the plane $z=0$ is given by

$$\begin{aligned} &W(x_1,y_1,x_2,y_2,0) \\ &= f^*(x_1,y_1)f(x_2,y_2)A^*(x_1',y_1')A(x_2',y_2') \\ &\quad\times\exp\left[-\frac{(x_1-x_2)^2+(y_1-y_2)^2}{\sigma_0^2}\right] \\ &\quad\times\exp[\mathrm{i}m(\arctan(y_2'/x_2')-\arctan(y_1'/x_1'))]. \end{aligned} \quad (14)$$

Now we consider that the background is a Gaussian beam

$$f(x,y)=\exp[-(x^2+y^2)/w_0^2] \quad (15)$$

with w_0 being the waist width, and the vortex core function takes the form

$$A(x',y')=(\sqrt{x'^2+y'^2}/w_0)^{|m|}. \quad (16)$$

For the sake of concreteness, we assume $m=-1$ and $\boldsymbol{d}=(d,0)$. So the cross-spectral density of GSM beam with vortex core at the plane $z=0$ can be expressed as

$$\begin{aligned} &W^{(1\mathrm{G})}(\boldsymbol{r}_{10},\boldsymbol{r}_{20},\omega) \\ &= \left[\frac{(\boldsymbol{r}_{10}-d)(\boldsymbol{r}_{20}^*-d)}{w_0^2}\right]^{|m|}\exp\left(-\frac{\boldsymbol{r}_{10}^2+\boldsymbol{r}_{20}^2}{w_0^2}\right) \\ &\quad\times\exp\left(-\frac{|\boldsymbol{r}_{10}-\boldsymbol{r}_{20}|^2}{\sigma_0^2}\right). \end{aligned} \quad (17)$$

Substituting Eqs. (17) into Eqs. (4), (6), (8), and (10), we obtain the electric cross-spectral density and the degree of spectral coherence of the light field in the regions II and III, respectively.

When the opening factors (expressed as xs) of the aperture along the x_2 and y_2 axes tend to infinity, and equation (18) is substituted into Eq. (8), we can obtain

$$W^{(3)}(\boldsymbol{r}_{11},\boldsymbol{r}_{22})=\frac{\pi^2w_0^2\sigma_0^2[4f^2w^4+d^2(k^2w_0^4\sigma_0^2+4f^2(2w_0^2+\sigma_0^2))]}{\lambda^2(k^2w_0^4\sigma_0^2+4f^2(2w_0^2+\sigma_0^2))^2}\exp\left[-\frac{\mathrm{i}k}{2f}(x_1^2-x_2^2+y_1^2-y_2^2)\right]. \quad (18)$$

In order to test and verify the validity of the calculation by using the 1/3 rule method of Simpson integration (Simpson's rule) in Eq. (4), we first analyse the intensity distribution on the axis after a plane wave is incident into a circular aperture, with the wavelength of the incident beam being $\lambda=633$ nm and the radius of the circular aperture being 10λ. The result of this method and that in Ref. [17] are shown in Fig. 2. As can be seen, the two results are in excellent agreement in the variation of the axial irradiance with the propagation distance. It confirms the validity of the numerical method for evaluating the diffraction integral in this paper; that is, the method can efficiently calculate the diffraction field of the aperture in $z\geq 0$ region.

Suppose that a GSM beam with vortex passes through a rectangular aperture, whose half-width lengths along the x and y directions are a and b, respectively. The wavelength of the GSM beam is $\lambda=1.06$ μm, its waist width $w_0=1.0$ mm; half-widths of the aperture along the x and y directions are $a=0.5w_0$ and $b=0.6w_0$, respectively. The degree of spatial coherence of the incident beam is $\beta=[1+(w_0/\sigma_0)^{-2}]^{1/2}=0.6$, and the off-axis parameter $d=0.5w_0$. Study of the property of the light field at $x_1=0$, $y_1=0.1w_0$ is carried out on the observation screen.

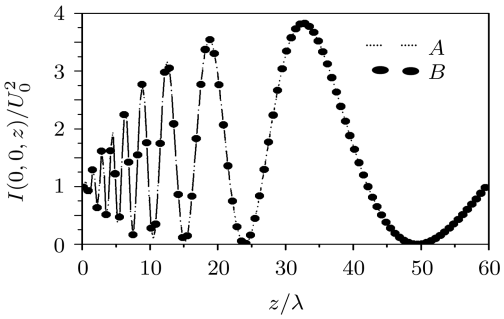


Fig. 2. The result in this paper in comparison with that in the literature. A corresponds to the result in this paper and B corresponds to the result in Ref. [17].

Figure 3 shows the spatial distribution of correlation vortices on the plane $z=4\lambda$ in the range of $x_2\in(-\lambda,\lambda)$, $y_2\in(-\lambda,\lambda)$ in the near-field diffraction region. As indicated in the figure, there exist 10 correlation vortices in the observation zone in total, and the spatial location of these correlation vortices is in a

grid-type distribution. Figure 4 depicts the distribution of these correlation vertices' phases. From Fig. 4, we find that the phases of these correlation vortices are undefined. Figure 5 shows the influence of the parameters z, β, d, and xs of the aperture on the location of the B correlation vortex. From Fig. 5(a), we find that the absolute value of the horizontal and longitudinal coordinates of B vortex point increases with increasing propagation distance. And this means that with increasing propagation distance, the vortex point moves outside the region $x_2 \in (-\lambda, \lambda)$, $y_2 \in (-\lambda, \lambda)$. This may be explained by employing the broadening effect of the aperture diffraction in a light field. Figure 5(b) reveals that the influence of β on the values of the horizontal (x_2) and longitudinal (y_2) coordinates are different. As shown in this figure, y_2 increases slowly with increasing β, and the oscillation amplitude changes no more than 0.5λ, while x_2 first increases dramatically in the range of $\beta \in (0, 0.5)$, and then decreases slowly in the range of $\beta \in (0.5, 1.0)$, while the oscillation amplitude is more than 1.5λ. From Fig. 5(c), we can see that the effect of the opening factor (xs) of the aperture along the x_2 axis on the spatial location (x_2, y_2) is opposite to that of β on the location of B vortex. The effect of the opening factor (xs) of the aperture along the y_2 axis on the spatial location of B vortex is similar to that in Fig. 5(c). Figure 5(d) shows the effect of the off-axis displacement d on the spatial location of B vortex. As is shown, the effect is relatively small, and the change of the spatial coordinates of the B vortex is small with increasing d.

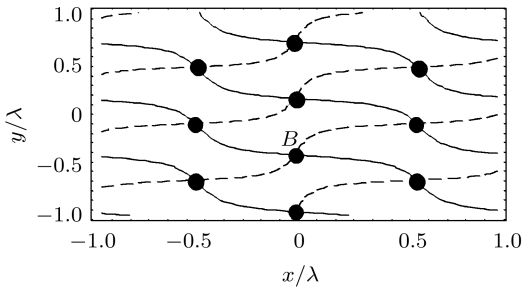


Fig. 3. Distribution of the coherent vortex at the propagation distance $z = 4\lambda$ in the range $x_2 \in (-\lambda,\lambda)$, $y_2 \in (-\lambda, \lambda)$.

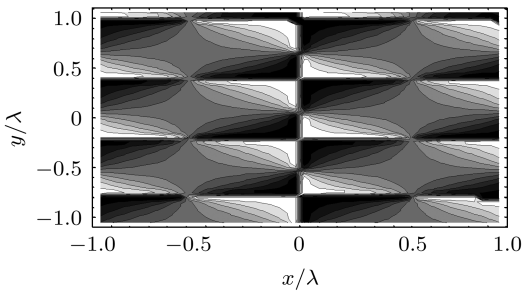


Fig. 4. Distribution of the correlation phase at propagation distance $z = 4\lambda$ in the range $x_2 \in (-\lambda, \lambda)$, $y_2 \in (-\lambda, \lambda)$.

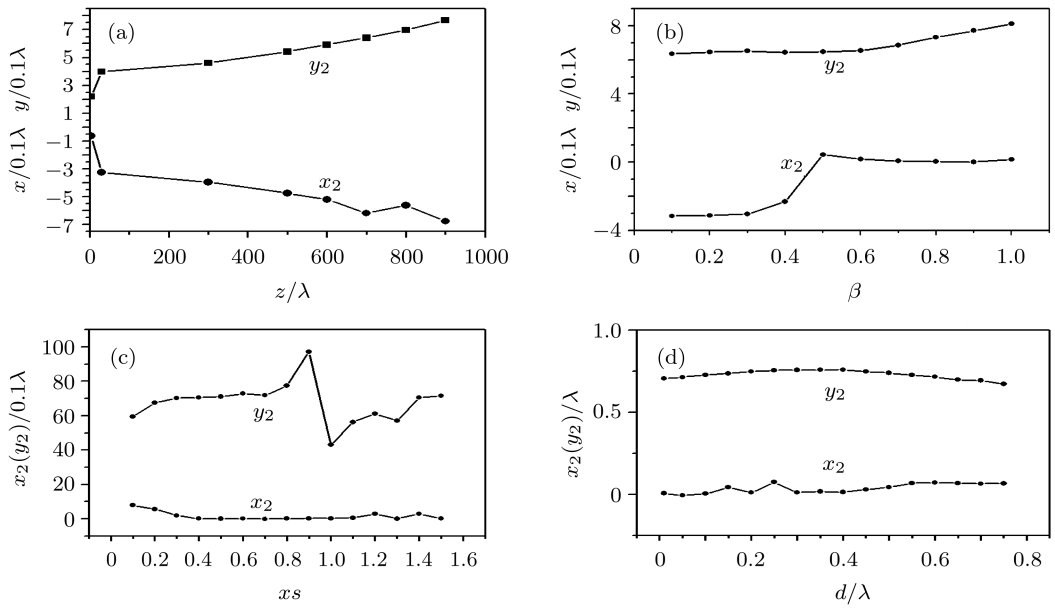


Fig. 5. Variation of the location (x_2, y_2) of B vortex point shown in Fig. 3 with the parameters: z, β, d and the opening factor (xs) along x direction of the aperture.

Figure 6 shows the variation of number of the vortex in the region of $x_2 \in (-\lambda, \lambda)$, $y_2 \in (-\lambda, \lambda)$ on the observation plane with the propagation distance z. As indicated, the number is decreased with increasing z. When the propagation ranges are $z \in (3\lambda, 70\lambda)$, $z \in (70\lambda, 800\lambda)$ and $z \in (800\lambda, 1500\lambda)$, their corresponding vortex numbers are 15, 6 and 1, respectively. This may come from the increasing broadening effect of the aperture diffraction due to the incident field with increasing propagation distance. Thus it will lead to the vortex points removing away from the propagation axial direction when the propagation distance increases, and the vortex number decreases to zero.

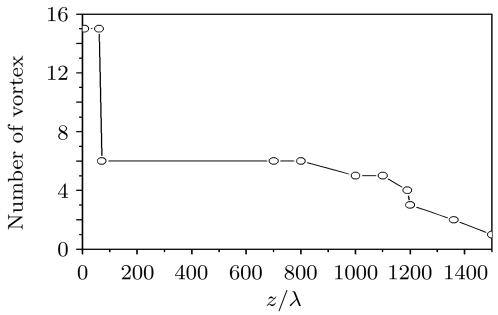


Fig. 6. Variation of the number of the vortex in region of $x_2 \in (-\lambda, \lambda)$, $y_2 \in (-\lambda, \lambda)$ in region II at $z = 4\lambda$ with propagation distance.

Figures 7 and 8 show the distribution of spectral degree of coherence of the diffraction field in region II and its variation along the $x_2(y_2)$ axis. As is shown, the distribution of spectral degree of coherence is not uniform across the plane of observation, and the variation trends along the x_2 and y_2 axes are similar. Now, we optimize the distribution of coherent vortex using the optimization algorithm. The result is shown in Fig. 9. The optimization parameters used are: $w_0 = 0.02$ mm; the half opening widths of the x and y axes are 0.1 and 0.2 mm, respectively; spatial degree of coherence parameter $\beta = [1 + (w_0/\sigma_0)^2]^{-1/2} = 0.6$, $\lambda = 1.06$ μm, and the off-paraxial displacement $d = 20\lambda$.

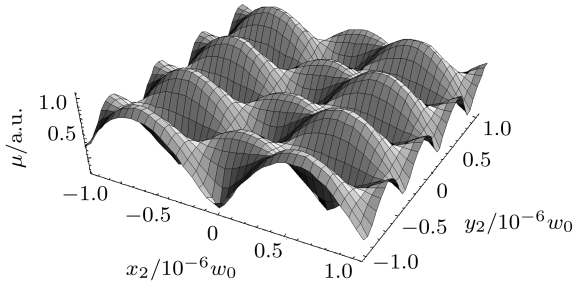


Fig. 7. Distribution of spectral degree of coherence in region II of the diffraction field.

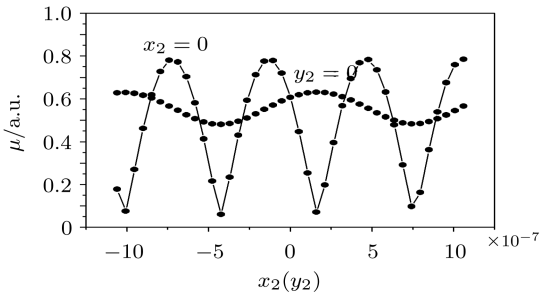


Fig. 8. Variation of spectral degree of coherence of the diffraction field in region II along the $x_2(y_2)$ axis.

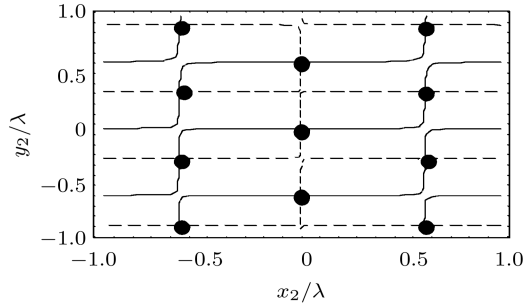
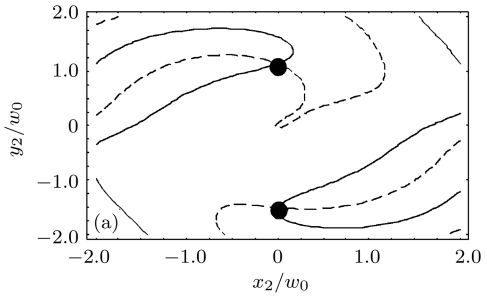


Fig. 9. Optimization distribution of the coherent vortex in the range of $x_2 \in (-\lambda, \lambda)$, $y_2 \in (-\lambda, \lambda)$ in region II.

Figure 10 illustrates the distribution of the correlation vortices and their contour phase diagram on the plane $z = 0.2$ m. As shown in Fig. 10, there exist two correlation vortices in the range of $x_2 \in (-2w_0, 2w_0)$ and $y_2 \in (-2w_0,\ 2w_0)$, their phases are undefined. Figure 11 shows the distribution of Re $(\mu_{xy}) = 0$ and Im $(\mu_{xy}) = 0$ in the range of $x_2 \in (-2w_0,\ 2w_0)$ and $y_2 \in (-2w_0,\ 2w_0)$ on the plane $z = 0.2m$ in the convergent region of lens whether the aperture is under the condition of $s_0 = 0$, Re $(\mu_{xy}) = 0$ and Im $(\mu_{xy}) = 0$. From Fig. 11, we find that there exists no cross-point of the real and imaginary parts of the spectral degree of coherence in the observing range. This means that the optical vortex has been destroyed by the convergent lens. The result that the aperture does not exist, can be explained by Eq. (14). From Eq. (18), it is found that the spectral degree of coherence of the diffraction field in the convergent region of lens is more than zero under the conditions in Fig. 10.



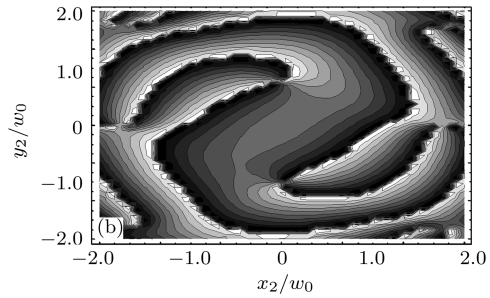


Fig. 10. Distribution and phase contour of correlation vortices in the range of $x_2 \in (-2w_0, 2w_0)$, $y_2 \in (-2w_0, 2w_0)$ on the plane $z = 0.2\ m$ in region II.

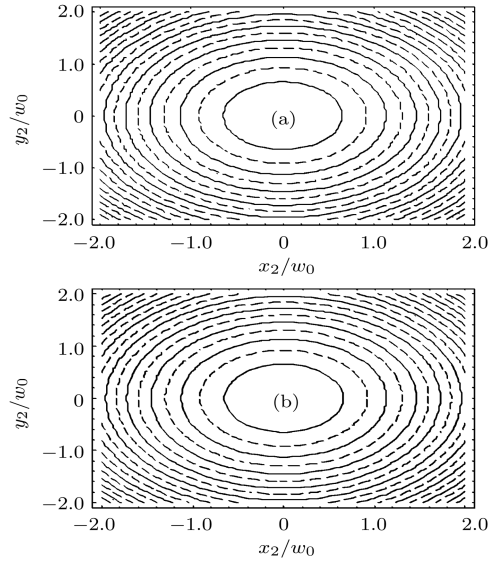


Fig. 11. Distribution of Re $(\mu_{xy}) = 0$ and Im $(\mu_{xy}) = 0$ in the range of $x_2 \in (-2w_0, 2w_0)$, $y_2 \in (-2w_0, 2w_0)$ on the plane $z = 0.2\ m$ in the convergent region of lens when $s_0 = 0$, (a) no aperture, (b) with an aperture.

4. Conclusion

We have derived the general expressions for the cross-spectral density of coherent vortex beams in the near-field diffracted by an arbitrary aperture, and for the cross-spectral density of the diffraction coherent vortex beams in the convergent region of the lens, illuminated by a GSM vortex beam diffracted by a rectangular aperture. We found that, in general, the spectral degree of coherence is not uniformly distributed over the plane of observation, and the convergent lens destroys the structure of the optical vortex. The numerical calculations show that the propagation distance z, off-paraxial displacement d, opening factors xs of the x_2 and y_2 axes and the spatial degree of coherence parameter β have different influences on the locations of the correlation vortices. Among the parameters stated above, we found that the influence of the propagation distance z is the greatest. At the same time, we have optimized the distribution of the correlation vortices on the observation plane by the optimization algorithm.

Acknowledgment

The author wishes to thank Dr. K. Cheng for fruitful discussions.

References

[1] Nye J F and Berry M V 1974 *Proc. R. Soc. Lond.* A **336** 165

[2] Soskin M S and Vasnetsov M V 2001 *Prog. Opt.* **42** 219

[3] Gbur G, Visser T D and Wolf E 2001 *Phys. Rev. Lett.* **88** 013901

[4] Foley J T and Wolf E 2002 *J. Opt. Soc. Am.* A **19** 2510

[5] Cheng K and Lu B D 2009 *J. Mod. Opt.* **56** 1119

[6] Schouten H F, Gbur G, Visser T D and Wolf E 2003 *Opt. Lett.* **28** 968

[7] Fischer D G and Visser T D 2004 *J. Opt. Soc. Am.* A **21** 2097

[8] Liu P S and Lu B D 2008 *Chin. Phys.* B **17** 1752

[9] Swartzlander Jr G A and Hernandez-Aranda R I 2007 *Phys. Rev. Lett.* **99** 163901

[10] Li J L and Zhu S F 2010 *Chin. Phys.* B **19** 054203

[11] Liu P S and Lu B D 2007 *Chin. Phys.* **16** 411

[12] Mandel L and Wolf E 1995 *Optical Coherence and Quantum Optics* (Cambradge: Cambridge University Press)

[13] Luneburg R K 1966 *Mathematical Theory of Theory of Optics* (Berkeley: University of California Press)

[14] Mendlovic D, Zalevsky Z and Konforti N 1997 *J. Mod. Opt.* **44** 407

[15] Pozrikidis C 1998 *Numerical Computation in Science and Engineering* (Oxford: Oxford University Press)

[16] Freund I and Shvartsman N 1994 *Phys. Rev.* A **50** 5164

[17] Stone J M 1963 *Radiation and Optics* (New York: McGraw-Hill)